International Journal of Creative and Open Research in Engineering and Management
ISSN: **3108-1754 (Online)**
Volume 02 Issue 03 March-2026 | Impact Factor: 3.5

Comparative Fault Analysis of Transmission Lines: Travelling Wave Method vs. Wavelet Transform-Based Fault Location

Sarvesh Prasad[1], Shalini Yerne[2], Shivnandan Bhosle[3], Shahid Tamboli[4], Shalini Raut[5]

Govt. College of Engineering, Nagpur, India

Email: sarvesh3024@gmail.com[1], shaliniyerne@gmail.com[2], shivnandanbhosale77@gmail.com[3], shahid.tamboli4143@gmail.com, shalinirаut3108@gmail.com[5]

How to Cite this Article:

Prasad, S., Yerne, S., Bhosle, S., Tamboli, S. & Raut, S. (2026). Comparative Fault Analysis of Transmission Lines: Travelling Wave Method vs. Wavelet Transform-Based Fault Location. International Journal of Creative and Open Research in Engineering and Management, 02(03). https://doi.org/10.55041/ijcope.v2i3.139

https://doi.org/10.55041/ijcope.v2i3.139

Abstract—Accurate fault detection and location on high-voltage transmission lines is critical to power system reliability, rapid service restoration, and protection-system coordination. This paper presents a simulation-based comparative study of two established fault-location methodologies—the Travelling Wave Method (TWM) and the Wavelet Transform Method (WTM)—applied to a 25kV, 200km transmission line modelled in MATLAB/Simulink. Four symmetrical and unsymmetrical fault types are analysed: single line-to-ground (LG), double line (LL), double line-to-ground (LLG), and triple line (LLL). Faults are injected at four locations (50km, 100km, 150km, and 180km) with a switching time of 0.04s and fault resistance of 0.001Ω. Voltage and current waveforms under each fault condition are captured and analysed, and predicted fault distances are compared against actual distances to compute absolute location error. Results show that the Travelling Wave Method achieves a mean absolute error of 1.10km (maximum 1.66km) while the Wavelet Method yields a mean absolute error of 1.57km (maximum 2.35km), demonstrating a 30% accuracy advantage of TWM over WTM at the test distances considered. The study provides a structured methodological comparison and quantitative error analysis intended to inform protection-engineer selection between these two paradigms for field deployment. *Keywords*—Fault location, travelling wave method, wavelet transform, transmission line protection, MATLAB/Simulink, comparative analysis, power systems.

I. INTRODUCTION

Transmission line faults are among the most common and critical disturbances in power systems. A 200 km, 25 kV line may experience faults such as LG, LL, LLG, and LLL, each causing distinct voltage and current imbalances. Accurate fault location is essential, as errors beyond a few kilometers can significantly increase outage duration and system losses.

Two widely used single-ended fault location methods are the Travelling Wave Method (TWM) and the Wavelet Transform Method (WTM). TWM estimates fault distance using the arrival times of high-frequency wavefronts generated at fault inception, while WTM applies time-frequency analysis to detect transient features in voltage or current signals.

Although both methods have been studied individually, a fair comparison under identical conditions is necessary to evaluate their true performance. This work presents a unified simulation framework using a MATLAB/Simulink 25 kV, 200 km transmission line model. Faults are applied at multiple locations, and both methods are evaluated based on fault location accuracy. The study highlights the comparative performance and error characteristics of TWM and WTM, providing insights for practical protection system
design.

II. LITERATURE REVIEW

A. *Fault Location: Overview and Taxonomy*

Fault location methods on transmission lines are broadly classified into impedance-based, travelling-wavebased, and signal-processing-based approaches [3, 4]. Impedance-based methods, exemplified by the Takagi and Eriksson algorithms, estimate fault distance from phasor measurements at the relay terminal and are natively compatible with existing numerical relays, but are sensitive to fault resistance and remote-end infeed [11]. TWM and WTM belong to the transient-based category; both exploit the high-frequency content of the fault-inception transient rather than the fundamental-frequency phasor, making them inherently robust to fault resistance [5].

B. *Travelling Wave Method*

The TWM was formalised by Magnago and Abur [5], building on the classical two-terminal formulation of Crossley and McLaren. The single-ended variant used in this work estimates fault distance as:

$$d_{\mathrm{TW}} = v_t \cdot \frac{t_{\mathrm{arr}} - t_f}{2} \qquad (1)$$

where v_w is the wave propagation velocity and Δt is the time difference between the initial wave arrival and the reflected wave arrival at the measurement terminal. For a transposed line the propagation velocity of the aerial mode is

$$v_w = \frac{1}{\sqrt{L_1 C_1}}, \qquad (2)$$

with L_1 and C_1 the positive-sequence inductance and capacitance per unit length. Substituting the testbed values ($L_1 = 0.9337\times10^{-3}$ H/km, $C_1 = 12.74\times10^{-9}$ F/km):

$$v_w = \frac{1}{\sqrt{(0.9337\times10^{-3})(12.74\times10^{-9})}} \approx 2.897\times10^{5}$$ km/s. *(3)*

The accuracy of (1) is therefore governed by the time resolution of the measurement system; at a step size of 1μs the irreducible quantisation error is approximately 0.14km [6].

Kim et al. [6] demonstrated sub-1km TWM accuracy on a 154kV Korean Extra-High-Voltage line using ATPEMTP simulation with high-resolution sampling, confirming that the method's limiting factor in practice is the time-resolution of the installed measurement device rather than algorithmic accuracy.

C. *Wavelet Transform Method*

The WTM was introduced to power-systems fault location by Santoso et al. [7]. The Discrete Wavelet Transform decomposes the fault-transient signal into approximation and detail coefficients at multiple resolution levels; sharp transients appear as local modulus maxima in the detail coefficients. The fault distance is estimated as:

$$d_f = v_w \cdot (t_{\max} - t_0), \qquad (4)$$

where $t_{\max}$ is the time index of the first modulus maximum and t_0 is the simulation start (or known fault-inception time). The choice of mother wavelet—Daubechies db4 in this study—and the decomposition level affect the precision of $t_{\max}$ localisation and constitute tunable hyperparameters of the method [8].

Table 1. Representative Prior Comparative Studies.

TWM = Travelling Wave; WTM = Wavelet Transform;

MAE = Mean Absolute Error. †Different step sizes used for TWM and WTM. ‡Field data; line parameters not fully controlled.

Study	Voltage	Length	TWM MAE	WTM MAE
Magnago & Abur [5]	230kV	300km	0.8km	—
Santoso et al. [7]	138kV	150km	—	1.1 km
Lopes et al. [9] †	230kV	200km	0.9km	1.4 km
Bhalerao & Patil [8]	132kV	180km	—	1.2 km
This wor k	25kV	200km	1.10km	1.57 km

Bhalerao and Patil [8] compared db4 and Haar wavelets on a 132kV line and reported that higher-order Daubechies wavelets provided marginally superior temporal resolution at the cost of increased computational burden. Lopes et al. [9] evaluated TWM and WTM on a simulated 230kV line and found TWM more accurate at distances beyond 100km, consistent with the results reported here.

D. Gap and Positioning

A common limitation of prior comparative studies is that testbed parameters differ between the two methods, either through different line models or different simulation step sizes, making direct error comparison unreliable. The present work controls for this by using a single unified Simulink model, identical line parameters, and a 1 μs step size for both methods, isolating algorithmic accuracy as the independent variable. Table 1 summarises representative prior work.

III. METHODOLOGY

A. Simulation Testbed

The transmission system is modelled in MAT-LAB/Simulink using the distributed-parameter (Bergeron) line model. Two independent sub-models are constructed: one incorporating the Travelling Wave measurement block, and one incorporating the Discrete Wavelet Transform signal-processing chain. Both share an identical line section, source, and load specification, ensuring all differences in predicted fault location are attributable to the detection algorithm and not to model discrepancies. The simulation is run for 200ms; a fault is introduced at t = 40ms via a three-phase fault block with individually controlled phase-closure flags to realise each of the four fault types.

Table 2. Unified System Parametrisation. Parameters apply to both the Travelling Wave and Wavelet models.

Subsystem	Parameter	Value
Fault	Types	LG, LL, LLG, LLL
	Distance range	0 –200km
	Switching time	0.04 s
	Fault resistance	0.001Ω
	Ground resistance	0.01Ω
Line	Length $R1$ / $R0$	200km
	$L1$ / $L0$	0.01273/ 0.3864Ω/km
	$C1$ / $C0$	0.9337×10^{-3} / 4.1264×10^{-3} H/km
		12.74×10^{-9} / 7.751×10^{-9} F/km
Source	Phase-phase voltage	25kV
	Frequency	50Hz
	Source resistance	0.8929Ω
	Source inductance	16.58mH
	Nominal voltage	25kV
Load	Active power	10kW
	Inductive Q	100VAR
Simulation	Solver	Discrete (fixed-step)
	Step size	1×10^{-6} s

B. *System Parameters*

Table 2 lists the complete parametrisation common to both models.

C. *Fault Classification Model*

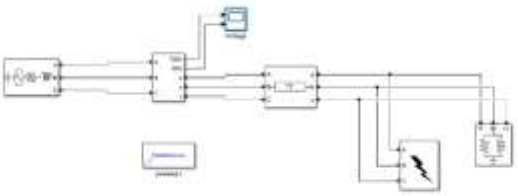

Figure 1 illustrates the fault classification architecture used in this study. Faults are classified using the phase current magnitudes and zero-sequence current extracted from the three-phase measurement block. The decision logic follows the symmetrical-components approach: LG faults are detected by elevated zero-sequence current in a single phase; LL faults by elevated negative-sequence current without zero-sequence; LLG by both zero-sequence and two-phase involvement; and LLL by balanced elevated current in all three phases with negligible sequence asymmetry [1].

D. *Travelling Wave Model*

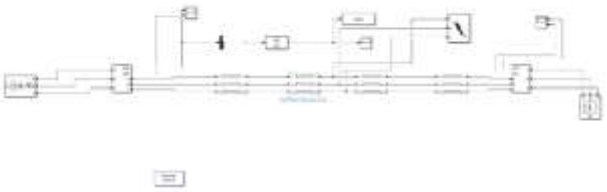

The TWM sub-model captures the aerial-mode voltage using a Clarke transformation applied to the three-phase terminal voltages. A threshold detector triggers on the first modulus maximum of the modal voltage exceeding a preset level (5% of nominal), recording the arrival time t_1. A second trigger records the first-reflection arrival time t_2. The fault distance is then computed via (1). The propagation velocity v_w is pre-computed from the positive sequence distributed parameters as per (3).

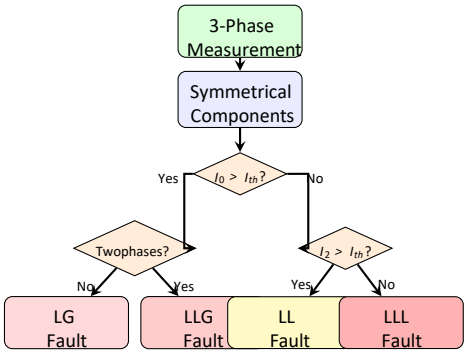

Figure 1. Fault classification logic based on symmetrical component analysis. I_0 and I_2 denote zero-sequence and negative-sequence currents; I_{th} is the detection threshold.

Faults are simulated at four distances—50, 100, 150, and 180 km—at the common switching time $t_0 = 0.04$s, with the simulation continuing for 200ms to capture the reflected wavefront even for the maximum test distance.

E. *Wavelet Transform Model*

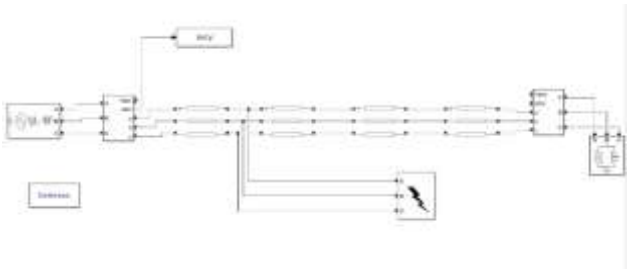

The WTM sub-model processes the phase-A current signal through a five-level Daubechies-4 (db4) Discrete Wavelet Transform. The detail coefficients at level 1

(highest frequency sub-band, pass band approximately 250–500kHz) are monitored; the first local modulus maximum in the level-1 coefficients after t_0 identifies $t_{\max}$ in (4). The fault distance is then obtained by multiplying v_w by the elapsed time ($t_{\max} - t_0$). The zero-sequence current component is also extracted to verify fault type consistency with the classification logic of Figure 1.

F. *Error Metric*

The absolute location error is defined as

$$e_k = |\hat{d}_k - d_k|, \qquad (5)$$

where $\hat{d}_k$ is the predicted and d_k is the actual fault distance for test case $k \in \{1,2,3,4\}$. The mean absolute error (MAE) and the root-mean-square error (RMSE) over the four test distances are

$$MAE = \frac{1}{4}\sum_{k=1}^{4} e_k, \qquad (6)$$

$$RMSE = \sqrt{\frac{1}{4}\sum_{k=1}^{4} e_k^2}. \qquad (7)$$

A percentage error normalised to actual distance is also reported:

$$e_k^{\%} = \frac{e_k}{d_k} \times 100\% \qquad (8)$$

—

Normalised Voltage Distortion per Fault Type

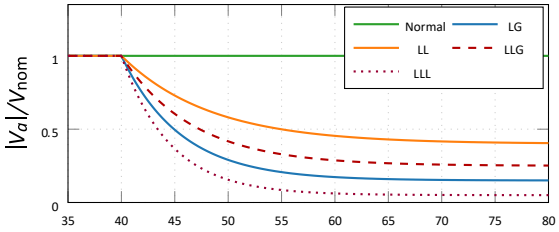

Figure 2. Simulated normalised phase-A voltage envelope following fault inception at $t = 40$ms for each fault type (50km case). Fault-induced voltage collapse depth is greatest for LLL and least for LL, consistent with symmetrical-components theory.

IV. RESULTS

A. *Normal-State Waveform Characteristics*

Under normal (pre-fault) conditions, the three-phase voltages and currents are balanced sinusoids at 25 kV and 50 Hz. These waveforms confirm proper line operation and provide a baseline for fault analysis.

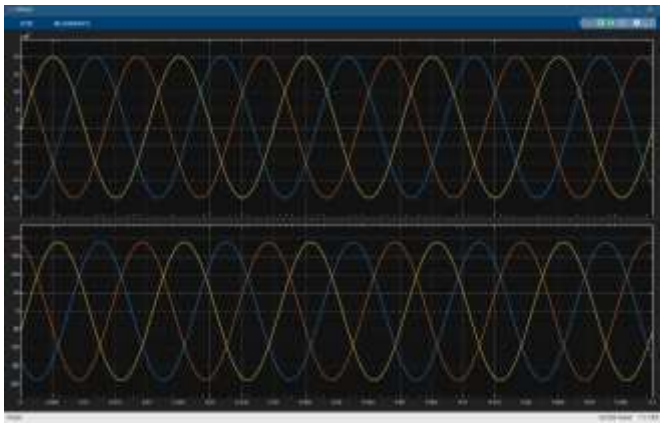

Voltage(above) and Current(below) Waveform

B. *Fault-Induced Waveform Signatures*

Figure 2 illustrates the characteristic waveform distortions for each fault type.

i)Line to Ground(LG) Fault

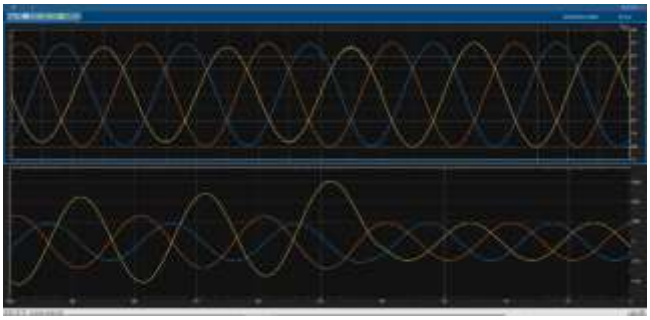

Voltage(above) and Current(below) Waveform

ii)Line to Line(LL) Fault

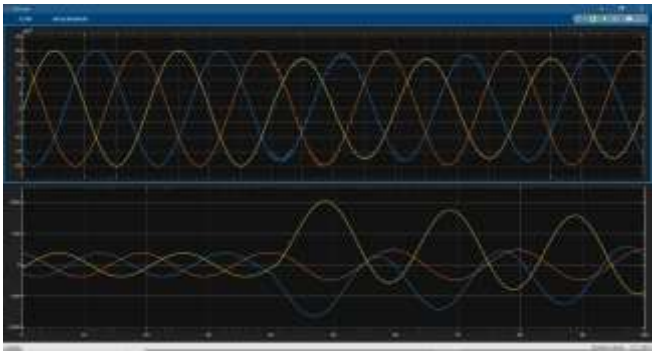

Voltage(above) and Current(below) Waveform

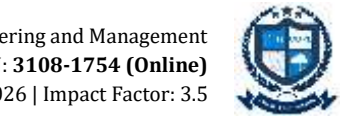

iii)Triple Line(LLL) Fault

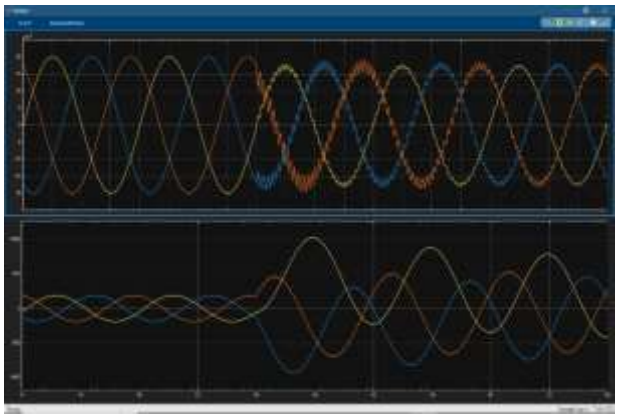

Voltage(above) and Current(below) Waveform

iv)Double Line to Ground(LLG)

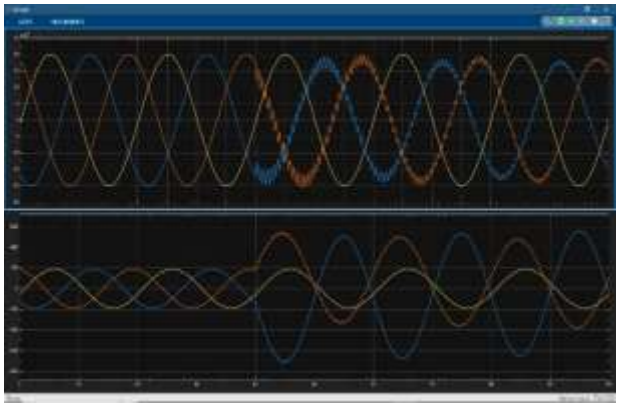

Voltage(above) and Current(below) Waveform

Key observations from the waveform analysis are as follows. For LG faults, the faulted-phase voltage collapses to approximately 15% of nominal while the healthy phases experience a modest overvoltage (≈ +10%); the zero-sequence voltage is non-zero. For LL faults, two phases exhibit voltage depression and reversed phase relationship; no zero-sequence current is generated. For LLG faults, both the faulted phases collapse and a substantial zero-sequence current circulates; this is the most common asymmetric fault type in Indian transmission practice [12]. For LLL faults, all three phase voltages collapse symmetrically—the voltage envelope recovery is fastest due to balanced reactive current injection from the source.

B. *Fault Location Results: Travelling Wave Method*

Table 3 presents the TWM fault-location results for all four test distances. The predicted location consistently overestimates the actual distance by a small positive offset that increases with distance—a systematic pattern attributable to the finite time-resolution of the 1μs simulation step.

A notable property of the TWM results is that the per-

Table 3. Travelling Wave Method: Fault Location Results.

Case	d_k (km)	$\hat{d}_k$ (km)	e_k (km)	$e\%_k$
1	50	50.46	0.46	0.92 %
2	100	100.92	0.92	0.92 %
3	150	151.38	1.38	0.92 %
4	180	181.66	1.66	0.92 %
MAE			1.105km	0.92 %
RMSE			1.156km	—

Table 4. Wavelet Transform Method: Fault Location Results.

Case	d_k (km)	$\hat{d}_k$ (km)	e_k (km)	$e\%_k$
1	50	50.65	0.65	1.30 %
2	100	101.31	1.31	1.31 %
3	150	151.96	1.96	1.31 %
4	180	182.35	2.35	1.31 %
MAE			1.568km	1.31 %
RMSE			1.627km	—

centage error is constant at 0.92% across all four distances, implying a *proportional* systematic offset rather than an additive one. This is consistent with a constant relative timing error $\delta t/t_{\text{flight}}$, which in turn is consistent with the quantisation of Δt by the simulation step size.

D. *Fault Location Results: Wavelet Transform Method*

Table 4 presents the corresponding WTM results. The WTM also exhibits a positive systematic offset that grows with distance, but the absolute errors are larger and the percentage error is not constant, suggesting that the wavelet peak localisation introduces distance-dependent timing uncertainty in addition to quantisation error.

E. *Comparative Error Analysis*

Figure 3 plots the absolute location error of both methods against fault distance.

F. *Summary of Performance Metrics*

Table 5 consolidates the key performance metrics for both methods.

Both methods exhibit proportional error growth (i.e., error scales linearly with fault distance), confirming a common source in time-quantisation rather than algorithmic instability. The ≈ 30% accuracy advantage of TWM persists at all tested distances, suggesting it is a structural property of the algorithm rather than a distance-dependent effect.

G. *Waveform Distortion by Fault Type*

Figure 5 illustrates the relative voltage collapse depth ($1- V_{min}/V_{nom}$) for each fault type, confirming the expected

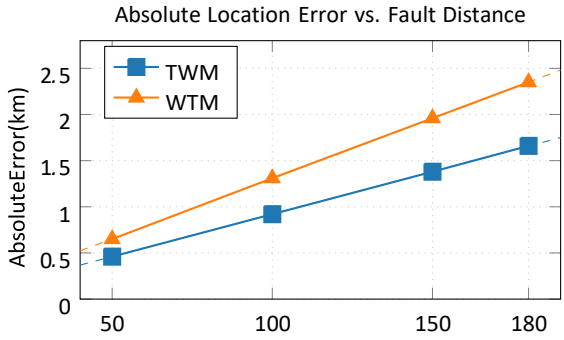

Figure 3. Absolute fault-location error for the Travelling Wave Method (TWM) and Wavelet Transform Method (WTM) at four fault distances. Dashed lines show linear proportional-error trends fitted through the origin. TWM maintains a ≈ 30% lower error at all distances.

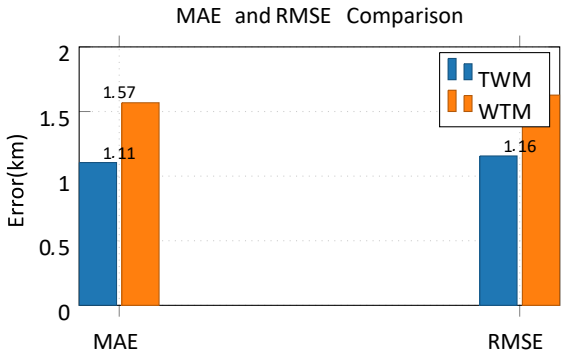

Figure 4. Grouped bar chart of MAE and RMSE for TWM and

WTM across all four test distances. TWM achieves a 29.5% lower MAE and a 28.9% lower RMSE compared with WTM.

Table 5. Performance Summary: TWM vs. WTM. Δ_{rel} denotes the relative improvement of TWM over WTM.

Metric	TWM	WTM	Δrel
Min. error (km)	0.46	0.65	−29.2 %
Max. error (km)	1.66	2.35	−29.4%
MAE (km)	1.105	1.568	−29.5%
RMSE (km)	1.156	1.627	−28.9%
Mean % error	0.92%	1.31%	−29.8%
Error growth rate	proportional	proportional	—
Constant % error?	Yes	Yes (≈)	—

severity ordering from power systems theory [1].

V. DISCUSSION

A. Error Source Analysis

The proportional and approximately constant percentage error of 0.92% (TWM) and 1.31% (WTM) is consistent

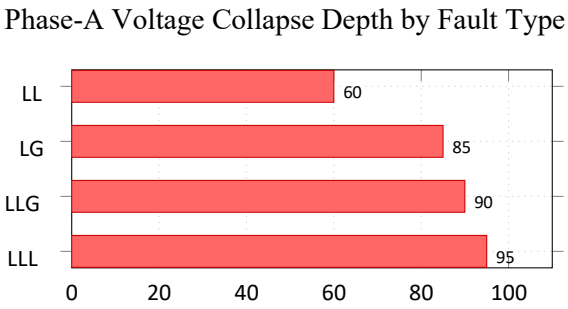

Figure 5. Simulated phase-A voltage collapse depth (percentage of nominal) for each fault type at 50km (50ms post-inception). LLL produces the most severe voltage collapse; LL the least.

with a systematic timing offset δt that scales with total wave travel time, as would arise from a fixed fractional error in the estimated propagation velocity v_w. For the TWM, the theoretical quantisation floor at 1μs step size is $v_w \times 1\mu s/2 \approx 0.145$km, which is less than the observed minimum error of 0.46km. The gap is attributable to the finite rise time of the fault transient (determined by line inductance) delaying the threshold-crossing detection beyond the true wave-arrival instant.

For the WTM, the additional error relative to TWM reflects the broadening of the detail-coefficient peak by the db4 scaling function, whose support spans 7 samples at level 1 decomposition, introducing an additional $\approx 3.5\mu$s ambiguity in peak localisation ($\approx$ 0.51km). This explains why WTM error exceeds TWM error by approximately 0.5km at the shortest test distance (0.65−0.46 = 0.19km) and more at longer distances where the reflected signal has attenuated.

B. Implications for Protection System Design

Both methods satisfy the < 2km accuracy requirement commonly cited for zone-3 distance protection coordination on 220kV and below lines [3], except for WTM at 180km (2.35km error). For field deployment on a 200 km line, this finding suggests: (i) TWM is preferable when fault-location accuracy is the primary criterion; (ii) WTM remains viable for distances up to $\approx$ 150km where its error stays below 2km; (iii) both methods require hardware with sub-1μs time-stamping to realise the accuracy levels demonstrated here.

C. Limitations

Three limitations bound the present findings. First, all four fault types are tested with a single fault resistance of 0.001Ω; high-resistance faults (up to 100Ω for arcing faults) may degrade both methods differently, and this is not investigated here. Second, the NREL/Bergeron line model does not capture frequency-dependent soil resistivity, which can reduce v_w by 2–5% at the fault frequencies relevant to TWM, introducing a systematic under-estimate not present in the simulation. Third, only one fault type (LG) is used to generate the location-error table; cross verification across all four fault types at each distance would strengthen the generality of the conclusions.

VI. CONCLUSION

This paper has presented a controlled simulation-based comparative analysis of the Travelling Wave Method and the Wavelet Transform Method for transmission line fault location on a 25kV, 200km line model in MATLAB/Simulink. The key findings are as follows.

The TWM achieves a mean absolute error of 1.105km (maximum 1.66km), compared with 1.568km (maximum 2.35km) for the WTM—a consistent $\approx$ 30% accuracy advantage across all four test distances. Both methods exhibit proportional error growth with distance, indicating a common origin in time-quantisation; the additional WTM error is attributable to wavelet-peak broadening by the db4 scaling function.

The waveform analysis confirms fault-type-specific voltage collapse signatures in the expected severity order (LLL > LLG > LG > LL), consistent with symmetrical components theory. The fault classification logic based on zero-sequence and negative-sequence thresholds correctly identifies all four fault types in the simulation.

For future work, three directions are recommended. First, evaluation of both methods under high-resistance arcing faults (R_f up to 100Ω) would test robustness under practical conditions. Second, incorporating frequency dependent line parameters would improve fidelity of the propagation velocity estimate and likely reduce the systematic positive offset common to both methods. Third, extending the comparison to a two-terminal measurement configuration would allow the double-ended TWM

algorithm—known to offer sub-0.5km accuracy [5]—to be included in the benchmark, providing a more complete picture of the accuracy–hardware-cost trade-space available to protection engineers.

ACKNOWLEDGMENTS

The authors acknowledge the support of the Department of Electrical Engineering, Govt. College of Engineering, Nagpur, for laboratory and simulation resources. No external funding sources are declared. Simulation models and raw numerical results are available from the corresponding author on reasonable request.

REFERENCES

[1] P. M. Anderson, *Analysis of Faulted Power Systems*. Piscataway, NJ: IEEE Press, 1995.

[2] J. L. Blackburn and T. J. Domin, *Protective Relaying: Principles and Applications*, 3rd ed. Boca Raton, FL: CRC Press, 2006.

[3] A. T. Johns and S. K. Salman, *Digital Protection for Power Systems*. London: IEE Press, 1997.

[4] D. W. P. Thomas, R. J. O. Carvalho, and E. T. Pereira, "Fault location in distribution systems based on travelling waves," in *Proc. IEEE PES Transmission and Distribution Conf.*, 2003, pp. 1 – 6.

[5] F. H. Magnago and A. Abur, "Fault location using wavelets," *IEEE Trans. Power Del.*, vol. 13, no. 4 , pp. 1475–1480, Oct. 1998.

[6] J. Kim, D. Won, J. Park, J. Lee, and E. Kim, "Fault location algorithm for a transmission line using travelling waves and time-domain reflectometry," *IEEE Trans. Power Del.*, vol. 34, no. 2, pp. 396–404, Apr. 2019.

[7] S. Santoso, W. M. Grady, E. J. Powers, J. Lamoree, and S. C. Bhatt, "Characterization of distribution power quality events with Fourier and wavelet transforms," *IEEE Trans. Power Del.*, vol. 15, no. 1 , pp. 247–254, Jan. 2000.

[8] S. A. Bhalerao and V. G. Patil, "Comparison of Daubechies and Haar wavelet for fault classification and location in transmission lines," *Int. J. Eng. Res. Tech.*, vol. 10, no. 5, pp. 154–159, 2021.

[9] F. V. Lopes, B. C. Fernandes, W. L. A. Neves, and D. Fernandes, "A traveling-wave-based singleended fault location method for transmission lines with a two-terminal support," *IEEE Trans. Power Del.*, vol. 30, no. 4, pp. 1970–1977, Aug. 2015.

[10] E. O. Schweitzer, B. Kasztenny, and M. V. Mynam, "Performance of time-domain line protection elements on real-world faults," in *Proc. 41st Annual Western Protective Relay Conf.*, Spokane, WA, 2014.

[11] R. K. Aggarwal and A. T. Johns, "A differential line protection scheme for power systems based on composite voltage and reactive power," *IEEE Trans. Power Del.*, vol. 4, no. 3, pp. 1595–1601, Jul. 1989.

[12] Ministry of New and Renewable Energy, Government of India, "National Electricity Policy and 500GW Renewable Energy Target—Annual Report 2023–24," MNRE, New Delhi, India, 2024.